VERIFICATION AND VALIDATION OF MONTE CARLO SIMULATIONS USING SWISS PWR HZP DATA

L. Berry (1), A. Vasiliev (1) *, M. Hursin (1), D. Rochman (1), M. Frankl (1), H. Ferroukhi (1)

(1) Paul Scherrer Institut, Forschungsstrasse 111, 5232 Villigen PSI, Switzerland
** Corresponding author email: alexander.vasiliev@psi.ch*

ABSTRACT

The use of Monte-Carlo (MC) simulations for reactor cores is currently of high interest [1][2]. Resulting MC models would be relevant, e.g., for high-resolution assessments of the local neutron flux and power gradients [3], generally beyond the modelling capabilities of deterministic codes for regular full core simulations. Such MC simulations would be of particular importance for the advancement of reactor operation and safety assessments or, for example, to support designing new materials testing experimental programs at operational reactors. Nevertheless, MC-based core-follow burnup calculations are still very challenging for routine applications. Therefore, the LRT/PSI has developed in recent years a "cycle-check-up" (CHUP) concept, which allows the transfer of the operating conditions (coolant and fuel temperatures, density of moderator, boron concentration, position of control rods) and burned fuel isotopic compositions from validated reference core-follow models, based on the state-of-the-art deterministic codes CASMO/SIMULATE/SNF to MC codes, such as Serpent or MCNP®. Thanks to the availability of the validated deterministic core-follow models and access to additional reference data for Swiss power plants, such as start-up tests at PWRs, there is a valuable opportunity to extend the validation database for criticality safety evaluation methodology using Swiss reactors data. This paper presents the ongoing work towards the verification and validation (V&V) of MC full core simulations for burned configurations against results of the validated deterministic models, as well as real measurements for hot zero power (HZP) reactor conditions.

KEYWORDS

Full core Monte Carlo simulation, spent fuel, verification and validation.

1. INTRODUCTION

Monte Carlo methods are commonly applied in neutron transport problems due to their unique capability in modelling complex three-dimensional systems and the use of neutron cross-sections with high resolution in the energy and angle variables. However, MC-based core-follow burnup calculations are still challenging for routine applications due to computationally requirements.

To overcome this limitation, a methodology consisting of loading information from validated burned deterministic models into an equivalent MC input is under development at PSI. For this purpose, the in-house automatic transfer tool COMPLINK [4] was used. The capability of this tool to automatically extend a user-given MC model to load heterogeneous material specifications, keeping track of the location of these materials within nested repeated structures, was used to model the core of a Swiss PWR at the beginning of a cycle (BOC), close to "equilibrium state". With this tool, the operating conditions and, most importantly, operational burned fuel isotopic compositions coming from CASMO-5/SIMULATE-3/SNF-1.07.05 were directly transferred in a MC input. By applying this methodology

on a PWR core MC template already available at PSI/LRT [5], a 38 million lines MC input was automatically created, accurately describing the HZP conditions at BOC.

To create these MC inputs, preliminary studies were necessary. Indeed, the drawback of the methodology used is the high memory consumption required for each simulation (up to 146 GB in the most extreme current case). By using this methodology in a brute force way, a single composition is defined for each of the 40 axial segments of every pin of the core. However, the core considered is composed of 177 fuel assemblies (FAs). Each of these FAs is composed of 205 pins and each of these pins is described axially by 40 segments. Therefore, a full-core simulation would require more than 1.4 million compositions, resulting in an extremely memory-intensive simulation.

Two approximations were made to address this problem. The first was to take advantage of the reactor "symmetries" to model only one octant of the core. The second solution was to realize a clustering of the pin compositions in the radial plane. For this purpose, the average composition of different pin groups was used to reduce the number of materials needed to describe each segment of the FAs.
For example, as shown in Figure 1, by using only the materials present in one octant of the core and repeating it over 360 degrees by reflection (using the USYM option of the Serpent 2.2 code), the number of FAs to be modelled was reduced to 29. In addition, an extreme clustering scheme has also been applied to this model. Only the average pin composition in each segment of the FA was modelled. With these two approximations, only $29 \times 40 \times 1 = 1160$ different compositions were needed to model the burned fuel. Finally, Serpent 2.2 was preferred over MCNP® 6.2 because of the memory consumption and initialization time of the simulations [6]. Using these approximations, it was possible to run the Serpent model shown on the right side of Figure 1 using only 10 GB of memory (see Section 4).

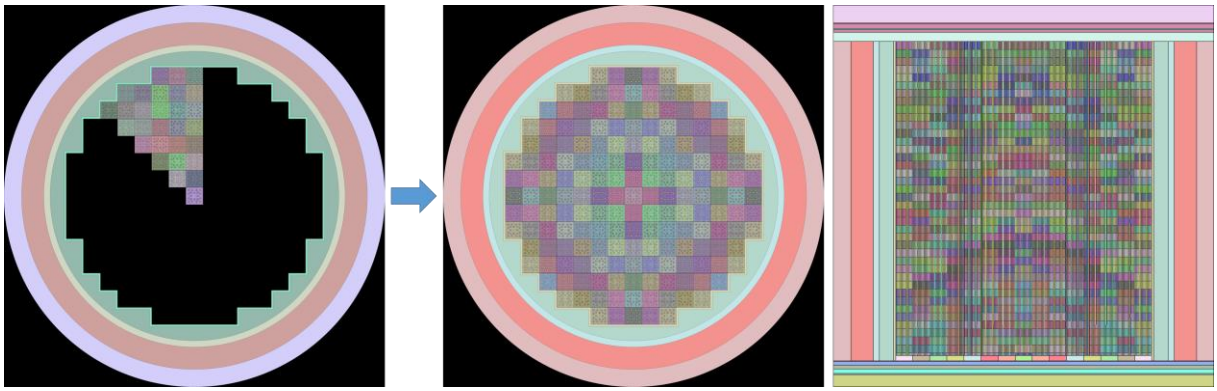

Figure 1. (Left) COMPLINK output. Serpent model: radial plane (Middle), axial plane (Right). One group of composition used per FA segment.

The work presented in this article consists of the V&V of the BOC MC model using a validated deterministic CASMO/SIMULATE scheme from which the isotopic composition is extracted using the SNF code [7]. Section 2 presents a verification of the isotopic composition produced by SNF against 13 isotopic weight fractions (wt. %) written in SIMULATE-3 (S3) output. Section 3 illustrates the verification of the k_{inf} of MC models for each of the 1160 segments that make up the core. Section 4 presents the validation of the full MC model using deviations from criticality and three-dimensional relative power fraction for different clustering schemes. The impact of the different clustering on memory consumption is also discussed in this section. Finally, Section 5 presents deviations from criticality of the MC model for a real experimental operating condition.

2. Verification of the fuel composition

A first verification of the mean isotopic composition of each FA was performed at BOC. Using the "PRI.ISO" card, S3 summarizes the weight fraction of 13 heavy metal isotopes for each FA. On the other hand, the SNF code can extract the isotopic concentration (in $\mathrm{g.tonHM^{-1}}$) of 680 isotopes for

each pin segment of each FA. The average SNF wt. % of each FA was then calculated and compared to those given by S3. Examples for U-235 and Am-241 are presented in Figure 2. It is important to note regarding Figure 2 that the 0% and "NA" relative deviations for U-235 and Am-241 correspond to fresh FAs. In fact, for the cycle considered, the FAs come from previous cycles and have thus specific Burnup values.

In the upper part of Figure 2, a good agreement is obtained for the fresh FAs. For these fresh FAs, the isotopic composition (U-234, U-235, U-236 and U-238) was manually extracted from the equivalent CASMO input. For the lower part, "NA" is specified, as no Am-241 is present in fresh FAs.

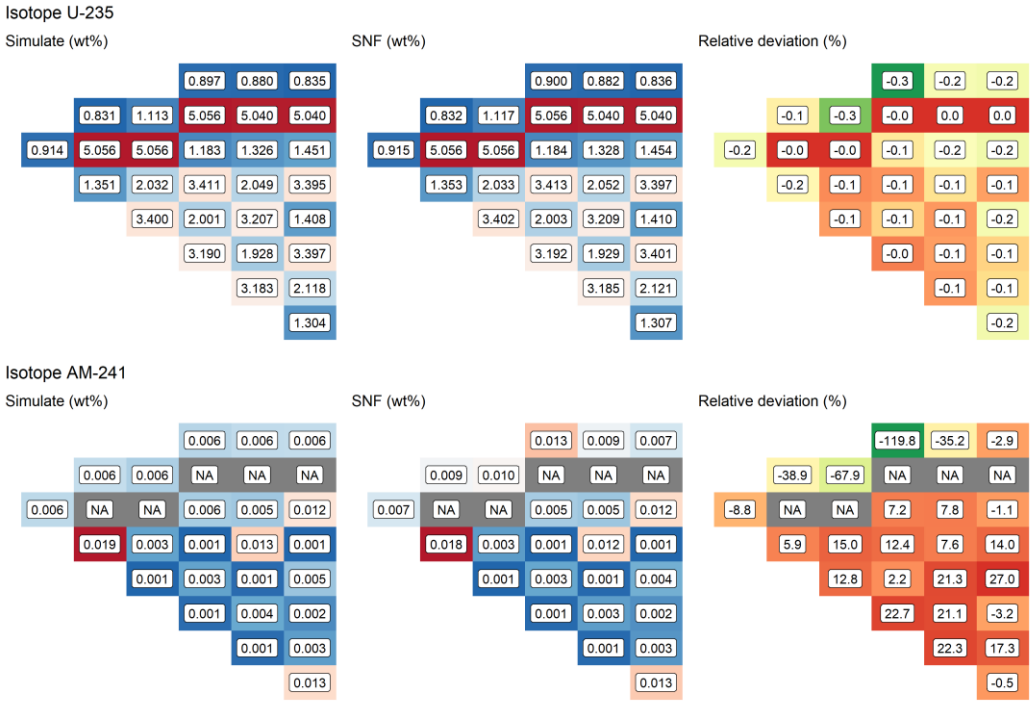

Figure 2. Axial-average fuel composition in wt. % given by S3 (left) and SNF (middle) for U235 (upper) and Am241 (bottom) and the relative deviations between these quantities (right).

It can be observed in the upper part of Figure 2, that the maximum relative deviation ($[S3 - SNF] \,/\, S3$) for isotope U-235 is -0.3%. Considering all FAs, the mean relative deviation for this isotope is -0.12% with a 0.09% standard deviation. The U-235 wt. % given by SNF can be considered in good agreement with S3. As shown in Table I, this agreement is similar for all other uranium isotopes.

Table I. Mean relative deviation between the isotopes given by S3 and SNF.

Isotope	Mean relative deviation $\pm$ 1 $sigma$ (%)	Isotope	Mean relative deviation $\pm$ 1 sigma (%)	Isotope	Mean relative deviation $\pm$ 1 sigma (%)
U-234	-0.26 $\pm$ 0.94	**Pu-238**	5.96 $\pm$ 9.63	**Np-237**	0.78 $\pm$ 0.95
U-235	-0.12 $\pm$ 0.09	**Pu-239**	-1.34 $\pm$ 2.88	**Am-241**	-2.57 $\pm$ 33.32
U-236	-0.01 $\pm$ 0.04	**Pu-240**	-1.15 $\pm$ 2.08	**Cm-242**	10.22 $\pm$ 33.31
U-238	-0.04 $\pm$ 0.03	**Pu-241**	0.44 $\pm$ 2.35	**Cm-244**	7.97 $\pm$ 13.12
		Pu-242	3.97 $\pm$ 7.05		

For the other isotopes, the agreement is not of the same quality. The mean relative deviations and variabilities are higher. For example, a mean deviation of 10% can be observed for Cm-242. Furthermore, when looking further at the compositions per FA, a relative deviation of -120% was

observed for isotope Am-241 (lower-right part of Figure 2). However, although the deviations are larger for these isotopes, the overall agreement between S3 and SNF was considered good enough.

3. k_{inf} numerical verification.

After verification of some isotopic compositions given by SNF, the next verification step was conducted on the most elementary bricks that make up the core. Independent MC models were constructed for each of the 1160 segments present in the octant of the core considered. For each of these models, all isotopes simultaneously present in the ENDF/B-VII.1 library and the SNF output were loaded. Thus, up to 244 isotopes were used to describe the composition of FAs segments. In practice, only 959 models were built. The first segment at the bottom of the core was not modelled due to geometrical inaccuracy. Similarly, not all 40 fresh FA segments were modelled (and a unique model was used), as they would have led to equivalent models (each of the 40 fresh FA segments share the same fuel composition).

The quantity used to verify these MC segment models is the infinite three-dimensional multiplication factor k_{inf} (3KIN card) given by S3. This quantity was compared to the effective multiplication factor (k_{eff}) given by the MC models using reflective conditions on all model outer boundaries, i.e. k_{inf}. To simplify the visualization of these results, the three-dimensional k_{inf} was averaged along the axial axis. This integration has led to the two-dimensional radial k_{inf}. This quantity is presented in the left-hand side of Figure 3 for S3 and the middle for the MC models (the first segment is not taken into account for the results presented in this section). These integrated MC results have a mean uncertainty of ± 3 pcm. The right-hand side of Figure 3 shows the difference between S3 and Serpents models.

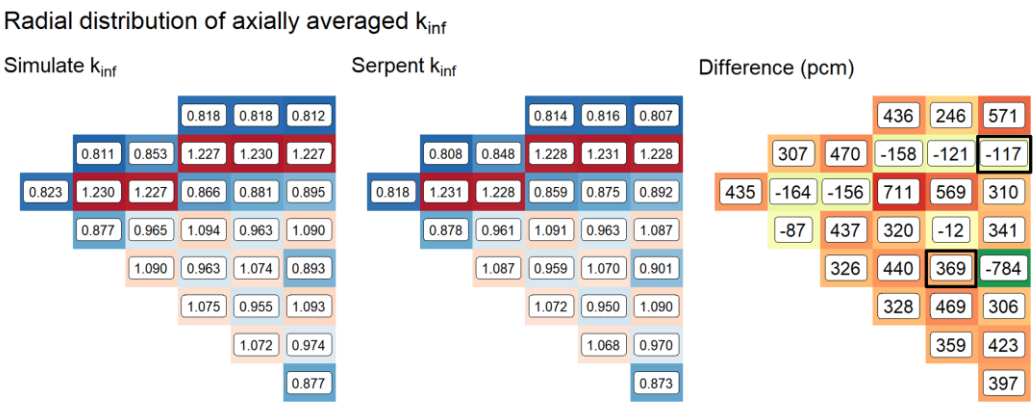

Figure 3. Radial distribution of axially averaged k_{inf}. Results from S3 (left) and Serpent (middle). (Right) Difference: ($S3 - Serp$)

Figure 3 shows good agreement between the axially averaged k_{inf} given by S3 and the Serpent models. For the 5 fresh FAs (assemblies with a $k_{inf} \approx 1.23$) a mean difference of -143 pcm is observed with a standard deviation of 22 pcm. For these FAs, the isotopic composition is exactly known, thus eliminating the uncertainty associated with its modelling. Thus, this result confirms that the geometry, compositions, and operation conditions of the FAs are well-modelled. For burned FAs, a mean difference of 320 pcm is observed with a standard deviation of 287 pcm.

To understand the behavior of these results, the axial node-wise distribution of the k_{inf} obtained for a fresh and burned FA is presented on the left and right side of Figure 4, respectively. The selected FAs are highlighted on the right-hand side of Figure 3 with a thick black frame. The fresh FA has an axially averaged k_{inf} difference of -117 pcm and the burned one has a +369 pcm difference.
Figure 4 presents the k_{inf} obtained for each of the independent MC models composing a FA. Segments 1-4 correspond to the bottom part of a FA. These segments include a dashpot zone to enhance structural

stability and to act as a shock absorber in case of rapid insertion of the control rods. Segment 5 corresponds to a segment with a dashpot at mid-height. Segments (6, 12, 18, 24, 30, and 36) include spacers and segments 38-40 include control rods. Remaining ones represent raw fuel segments.

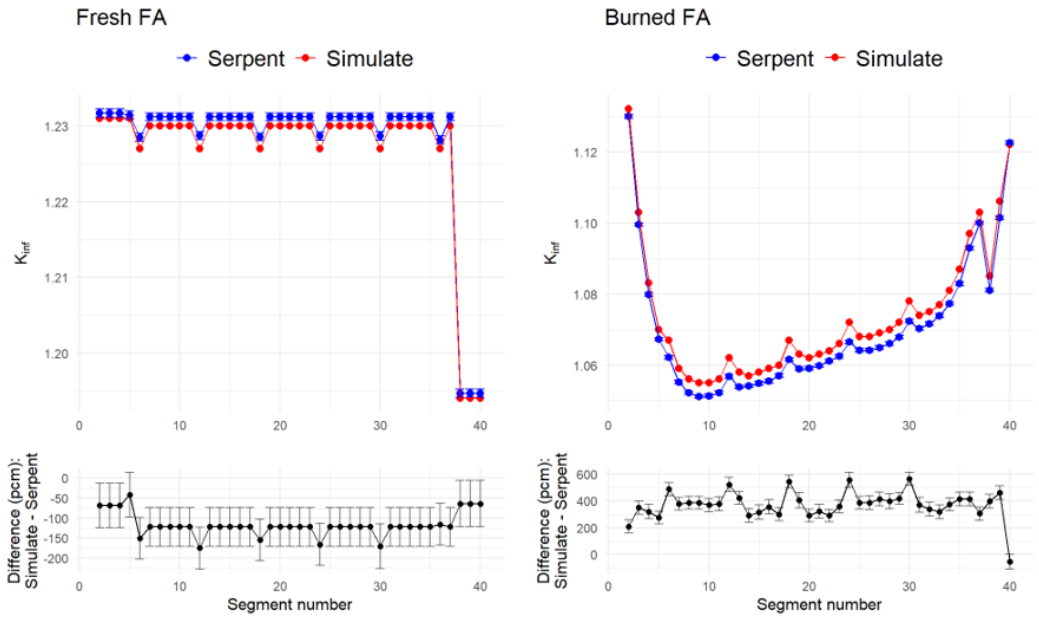

Figure 4. Axial node-wise k_{inf} distribution for a fresh (left) and burned (right) fuel assembly. Uncertainty given at $\pm 3\sigma$ for MC results.

The k_{inf} nodal distribution of the fresh FA displayed on the left of Figure 4 shows that a good agreement is obtained between Serpent and S3. A small Serpent overestimation is systematically observed (axially averaged k_{inf} difference of -117 pcm for this fresh FA). This figure gives thus some confidence in the MC modelling performed even if small differences are observed.

Concerning the burned FA nodal k_{inf} distribution shown on the right-hand side of Figure 4, a difference of about 400 pcm is obtained over the whole set of raw fuel segments. For the six spacer models, a difference of 600 pcm is obtained. This difference of 200 pcm compared to the raw segments means that the spacer models still need to be adjusted to match closer to the S3 results. Finally, segment 40 shows a significant difference from the other control rod segments 38 and 39 (as well as from all other FA segments). However, the MC model of segment 40 is equivalent to the other control rod models except for the SNF isotopic composition loaded. This discrepancy can be explained by the isotopic composition for segment 40, which may not be as good as for the other segments due to the proximity of the reflector.

Two weaknesses of the k_{inf} verification must be highlighted. First, with this quantity, it was not possible to verify the reflector of the MC model. No information on the reflector is contained in the k_{inf} results, which makes this verification unfeasible with this quantity. The second weakness is that only the average pin composition per FA and segment were used. This approximation was made to reduce the computational burden of this analysis. Each simulation took an average of 33 minutes on 7 tasks to achieve an uncertainty of 0.02% on the multiplication factor. Given that 1000 simulations were performed, this approximation was considered sufficient in a first verification phase.

As a conclusion to this section, even if some possible mismatches were identified, the overall agreement between the k_{inf} results given by Serpent and S3 was considered good enough at this stage of the work. To continue this study a k_{eff} and a relative power fraction (RPF) comparison over a full core MC model against S3 is presented in the next section.

4. k_{eff} numerical validation

In this section, full core simulations were considered using the compositions present in one octant of the core and repeating over 360 degrees by reflection. The effect of four different composition clustering schemes was studied on the neutron multiplication factor and memory consumption. It is well known [6] that the use of a large number of cells and compositions in a MC input has an impact on the size of the memory required to run a simulation. Given that the computational cluster used to run these simulations has 256 GB of RAM, four progressively more refined MC inputs were prepared to test the limits of achievable modelling and validated against a model using pin-wise composition.

The nuclear lattice of the FAs studied is described by a 15×15 grid composed of 205 nuclear fuel rods and 20 guide tubes. The first clustering scheme studied uses the most extreme approximation. The average fuel composition of each segment was loaded into all of the 205 fuel pins. Consequently, only 40 different fuel compositions were needed per FA. This clustering scheme is presented on the left side of Figure 5 (and also in Figure 1). The second clustering scheme prepared uses 9 groups of compositions per segment. For this model, a regular grid of 5×5 pins was used. The resulting clustering is displayed in the middle-left of Figure 5. The 25 groups clustering uses also a regular grid. This time a thinner grid step of 3×3 pins was used. The resulting mesh is displayed in the middle-right of Figure 5. Finally, the finest clustering scheme uses 81 groups. As shown on the right-hand side of Figure 5, this clustering uses an evolving grid step that is thinner near the edge and wider in the center of each FA.

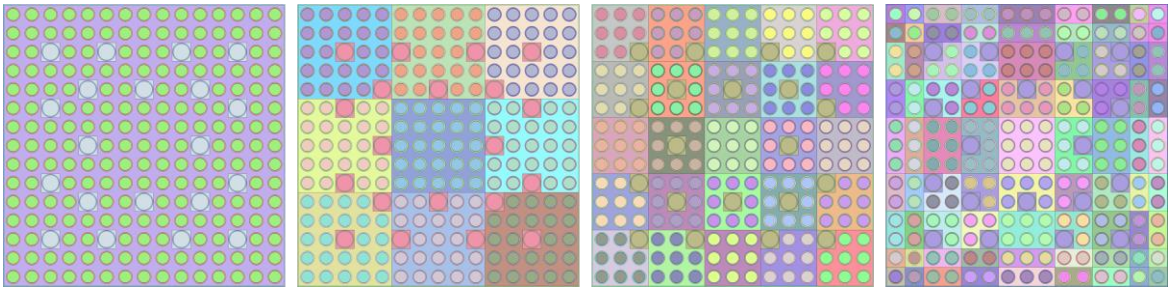

Figure 5. Clustering scheme. From left to right: 1, 9, 25 and 81 groups per FA and segments.

The creation of these Serpent MC models has been automated using the COMPLINK tool and its options (this tool can also create MCNP® models). Using this tool for the pin-wise composition model made it easy to create an input file of 38 million lines with the required fuel composition resolution, operating conditions, geometry, coolant and fuel temperature, moderator density, boron concentration and position of control rods. By using this tool, 252892 cells were created at the right place using 231742 well-defined materials. However, this high resolution is challenging. In practice, the automated creation of the pin-wise MC input (displayed in Figure 6) using this in-house tool has required 3.5 day.

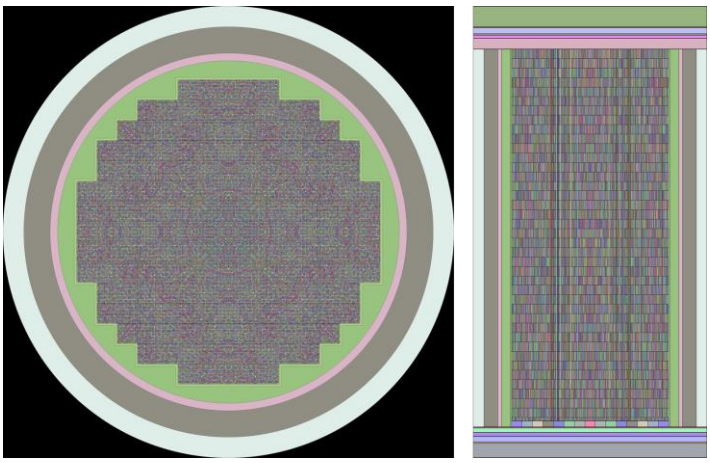

Figure 6. MC model using pin-wise composition for each segment of each assembly.

As expected, it can be observed in the column "RAM consumption" in Table II, that by increasing the number of groups (and consequently the number of cells and materials) memory consumption has significantly increased. A linear approximation of this trend, for the four models using the clustering approximation, would be that each group requires 1 GB of additional memory, knowing that the memory required for the 1–fuel rod group model is 10 GB. Looking at the result for the pin-wise composition model, it can be seen that the memory requirement is only 55 more GB than the 81-clustering scheme model. If the linear trend had been followed, 215 GB would have been needed for the pin-wise simulation.

In addition, it can be observed in the column "Difference k_{eff}" of Table II for the considered HZP operating condition, that the overall agreement for the multiplication factor provided by S3 (1.00000 as a matter of principle) and those from the MC models are in the range of 240-295 pcm. By using a thinner grouping scheme or even the pin-wise resolution, the multiplication factor moves away from criticality. However, the observed deviation range is quite small (51 pcm), meaning that as a first approximation, it may be interesting to work with the 1-group model. By doing so, it is possible to avoid the memory drawbacks of MC simulations and the time required to generate input models using the COMPLINK tool. With this clustering scheme, it takes only 1 minute to generate the input file composed of 260,000 lines. It can also be observed that the effect of the clustering approximation associated with the use of 81 groups leads to only a 3 pcm discrepancy in comparison to the pin-wise resolution simulation.

Table II. Effective multiplication factor validation for different clustering schemes.

Clustering scheme	Number of cells	Number of materials	RAM consumption	k_{eff} ($\pm\sigma_{\%}$) Serpent	Difference k_{eff} S3 - Serpent (pcm)
1	2337	1844	10 Gb	0.99759 ($\pm$0.001%)	241
9	12420	11154	18 Gb	0.99738 ($\pm$0.001%)	262
25	31871	29137	31 Gb	0.99724 ($\pm$0.001%)	276
81	98916	91122	91 Gb	0.99711 ($\pm$0.001%)	289
Pin-wise	252892	231742	146 Gb	0.99708 ($\pm$0.001%)	292

The numerical validation of the MC models is performed against S3. Therefore, a multitude of quantities can be extracted directly from the S3 output to validate the MC models. To complete the numerical validation, the 3D relative power fraction output of S3 (3RPF card) was also studied. The use of this three-dimensional information allows for a more accurate identification of the location of possible discrepancies in the modelling performed. To estimate this quantity with Serpent, total fission rates were tracked on a mesh covering each of the FAs segments. This information was then normalized to obtain the 3D RPF from the MC outputs.

An axial average was performed to ease the visualization of this three-dimensional quantity. The resulting 2D radial RPF distribution is displayed in Figure 7. The left side of Figure 7 presents the results extracted from S3, the middle side presents the results estimated with Serpent using the 81-group clustering scheme introduced previously and the right side presents the relative difference ($[S3 - Serp] / S3$) between these two quantities.

Qualitatively, a good agreement is obtained between S3 and Serpent for the radial distribution of axially average RPF with relative deviations in the $[-7\%, 7\%]$ range. A detailed examination of these deviations leads to several observations. First, S3 overestimates Serpent in the center of the core. Secondly, "discrepancy patterns" are repeated all over the core. These patterns are probably due to the octant approximation presented in Figure 1. By repeating the composition of the FAs present in a single octant over the entire core, asymmetries present in the real core and modeled with S3 are not taken into account in the MC model. This approximation can therefore lead to the observed discrepancy patterns. For example, the 4 highest observed relative deviations (6-7% deviations displayed in red on the right-

hand side of Figure 7) are associated with the 4 highest FA exposure asymmetries (in the center of the core).

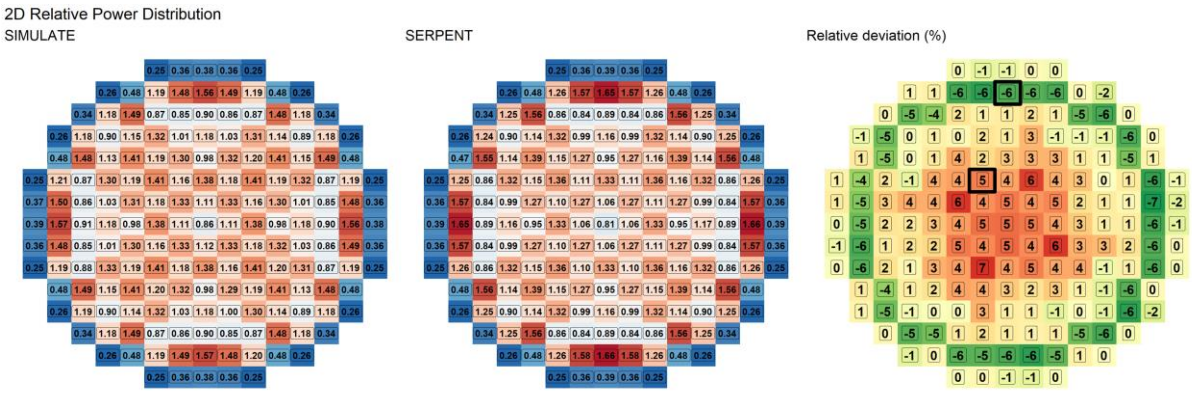

Figure 7. Radial distribution of axially averaged RPF estimate with S3 (left) and Serpent using the 81-group clustering scheme (middle). (Right) Relative deviation between these quantities in percent.

On the other hand, S3 underestimates Serpent in the core-periphery. This discrepancy is observed for all fresh FAs. The associated relative deviations are in the [-7,-4] % range and are shown in green on the right-hand side of Figure 7. However, good agreements were obtained in the numerical validation performed with the k_{inf} on fresh FAs (illustrated in the left-hand side of Figure 4). Therefore, the normalization of the fission rates estimated using Serpent to subsequently derive the 3D RPF may explain this discrepancy.

To complete these validation results, the radially averaged 3D RPF is displayed on the left-hand side of Figure 8. Good agreement is also observed with associated relative deviations in the [-8, 4] % range. A linear trend is observed for the relative deviation between segments 9-36. As with the axially averaged RPF, this observation may be due to the performed normalization. Another observation concerns segment 1 at the bottom of the core. The relative error of this segment is quite different from the neighboring segment 2. This difference may be due to the modelling of the bottom reflector in the current MC model. However, as the mean axial RPF curve shows (left of Figure 8), although the discrepancy is larger for this segment, the contribution to the core power is small. Consequently, this discrepancy can be considered as of the second order. Segment 40 also behaves differently from other segments. This segment is also located near top reflector. Therefore, due to the discrepancies observed near the reflector, a refinement of the MC model will be performed on the top and bottom part of the core to improve the argument with S3 outputs.

In addition to the mean axial RPF distribution, the node-wise RPF distribution of a fresh and burned FA is presented in the middle and right side of Figure 8. These two FAs are highlighted in Figure 7 by thick black borders. The fresh FA has a mean relative deviation of -6% and the burned one 5%. The overall profile of the relative deviation from these two FAs is similar to the average one. It can be observed in the middle graph of Figure 8, that Serpent systematically overestimates S3 for the fresh FA. For the burned FA, S3 overestimates Serpent by up to 10% at the top of the core.

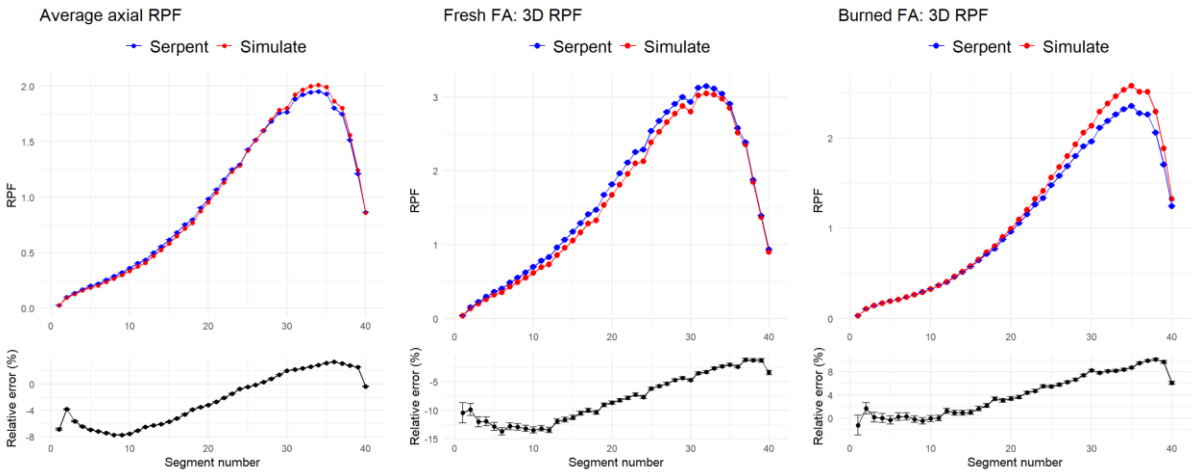

Figure 8. (Left) Axial distribution of radially average RPF. Axial node-wise RPF for a fresh FA (Middle) and a burned one (Right). Uncertainty given at $\pm 3\sigma$ for MC results.

5. k_{eff} experimental validation and perspectives

Following the numerical validation, an experimental validation was performed using measured HZP conditions. The measured boron concentration, temperature and position of the control rods were specified in the MC models. The octant composition approximation and the 1-group clustering scheme were used for the experimental validation. Using this model at this experimental operating condition, a 400 ± 1 pcm subcritical model was obtained. Given the results obtained in Table II, the use of the pin-wise composition resolution would probably result in a deviation of 450 pcm.

To push further this work different tasks will be considered. Looking at the numerical validation based on the relative power fraction, an idea would be to model more than an octant of the core. By doing so, discrepancies associated with asymmetries will possibly be corrected. However, the memory required by these simulations will significantly increase. Therefore, the number of groups that can be used for clustering will decrease as a larger portion of the core is modelled. To address this constraint, one possibility would be to develop a grouping scheme based on the spatial distribution of the isotopic composition of the burned FAs depending on the number of available groups. By using techniques that reduce the dimension of the problem while preserving the maximum amount of information, a more elaborated grouping scheme would be produced. First trials were realized using principal component analysis. By doing so, better informed clustering schemes were produced. This strategy will be automatized and verified on the octant MC model against available S3 results. It will then be possible to implement it on MC models of a larger portion of the core to tackle memory limitations.

It would also be interesting to identify the cause of the small discrepancies observed during the k_{inf} analysis presented in section 3 and to correct the doubtful top and bottom reflector. By doing so, the MC model would be even closer to the true operating core. Another idea would be to use SIMULATE-5 as a new reference for the numerical validation. It would be also interesting to perform the presented numerical validation on other operation conditions than the studied HZP condition. By studying more cases, better confidence will be obtained in the MC model created. As the COMPLINK tool has been specially developed to study hot full power, this idea seems feasible.

The final step of this V&V study would be to confront the MC model with experimental in-core measurements, as well as additional verification of the multiplication factor of other HZP operation conditions. These studies would give a strong validation of the modelling performed.

6. Conclusion

This article presents different analyses dedicated to the V&V of a MC model of an evolved HZP condition. Two approximations were presented to overcome the known memory limitations of this type of simulations. These approximations consist of a symmetry approximation and a clustering of pin compositions to reduce the number of materials required. Based on these approximations, a MC input composed of 231742 different materials was constructed using the in-house COMPLINK tool for the automatic generation of burned configurations. The fuel pin composition was extracted directly from SNF outputs associated with a validated deterministic model.

First, verification of these compositions was performed against S3. Secondly, the MC modelling was verified using the infinite multiplication factor of the simplest blocks making up the full core. A numerical validation was also conducted using the full core model against validated deterministic results. During this numerical validation, the impact of the clustering approximation was studied. Using pin-wise resolution, a 38 million line input was generated leading to simulations requiring 146 GB of memory. For this specific model, a 292 pcm deviation from criticality was observed. In addition to this validation, the three-dimensional power obtained with the MC model was also verified. Agreement in the [-6, 5] % range was obtained for the axially integrated power outputs. Finally, an experimental validation was performed for a real operating condition. A 400 pcm deviation from criticality was observed using a coarse clustering approximation. All these results show that the MC model can still be improved and validated using more precise approximations and more numerical and experimental results.

It should be noted that the obtained k_{eff} bias should be considered as preliminary and in the future accomplished with k_{eff} uncertainties evaluations associated with a) nuclear data uncertainties used for the criticality calculations and b) isotopic composition biases and uncertainties coming from CASMO/SIMULATE/SNF.

ACKNOWLEDGMENTS

The authors are grateful to Dr. Marco Pecchia for advancing this work at PSI at its initial stages.

7. References

[1] Goričanec, Tanja, et al. "Applicability of the Krško nuclear power plant core Monte Carlo model for the determination of the neutron source term." Nuclear Engineering and Technology 53.11 (2021): 3528-3542.
[2] García, Manuel, et al. "Validation of Serpent-SUBCHANFLOW-TRANSURANUS pin-by-pin burnup calculations using experimental data from the Temelín II VVER-1000 reactor." Nuclear Engineering and Technology 53.10 (2021): 3133-3150.
[3] Vasiliev, A., et al. "Localized neutron flux assessment and verification studies using MCNPX PWR full core model." Annals of Nuclear Energy 92 (2016): 317-332.
[4] Pecchia, M., et al. "Studies of intra-pin power distributions in operated BWR fuel assemblies using MCNP with a cycle check-up methodology." Annals of Nuclear Energy 129 (2019): 67-78.
[5] Pecchia, M., “Methodology for automatizing the representation of heterogeneous material dataset with temperature effects in large scale model”. Intern Report (2016).
[6] Hursin, M., et al. “Monte Carlo analysis of BWR geometries using a cycle check-up methodology.” To be published.
[7] Rochman, D., et al. “Consistent criticality and radiation studies of Swiss spent nuclear fuel: The CS2M approach”. Journal of Hazardous Materials 357 (2018): 384–392.